ADVANCED MATERIALS
www.advmat.de

Noncovalent Polymerization-Activated Ultrastrong Near-Infrared Room-Temperature Phosphorescence Energy Transfer Assembly in Aqueous Solution

*Xian-Yin Dai, Man Huo, Xiaoyun Dong, Yu-Yang Hu, and Yu Liu**

Noncovalent macrocycle-confined supramolecular purely organic room-temperature phosphorescence (RTP) is a current research hotspot. Herein, a high-efficiency noncovalent polymerization-activated near-infrared (NIR)-emissive RTP-harvesting system in aqueous solution based on the stepwise confinement of cucurbit[7]uril (CB[7]) and β-cyclodextrin-grafted hyaluronic acid (HACD), is reported. Compared with the dodecyl-chain-bridged 6-bromoisoquinoline derivative (G), the dumbbell-shaped assembly G⊂CB[7] presents an appeared complexation-induced RTP signal at 540 nm via the first confinement of CB[7]. Subsequently, benefitting from the stepwise confinement encapsulation of the β-cyclodextrin cavity, the subsequent noncovalent polymerization of the binary G⊂CB[7] assembly enabled by HACD can contribute to the further-enhanced RTP emission intensity approximately eight times in addition to an increased lifetime from 59.0 µs to 0.581 ms. Moreover, upon doping a small amount of two types of organic dyes, Nile blue or tetrakis(4-sulfophenyl)porphyrin as an acceptor into the supramolecular confinement assembly G⊂CB[7]@HACD, efficient RTP energy transfer occurs accompanied by a long-lived NIR-emitting performance (680 and 710 nm) with a high donor/acceptor ratio. Intriguingly, the prepared RTP-harvesting system is successfully applied for targeted NIR imaging of living tumor cells by utilizing the targeting ability of hyaluronic acid, which provides a new strategy to create advanced water-soluble NIR phosphorescent materials.

1. Introduction

Supramolecular macrocyclic-confinement artificial light-harvesting luminescent materials have received an increasing attention in recent years, which displayed ingenious applications in miscellaneous fields, such as bioimaging,[1] optical probes,[2] light-emitting materials,[3] and photochemical catalysis.[4] This light-harvesting process depends primarily on Förster resonance energy transfer (FRET) mechanism, where the energy transfers from excited singlet donors to singlet acceptors along with a corresponding high donor/acceptor ratio.[5] Generally, organic fluorescent molecules with aggregation-induced emission property are adopted as ideal donors to mitigate fluorescence quenching and guarantee the significant enhancement of fluorescence emission after forming noncovalent supramolecular assembly in aqueous media.[6] However, most of these reported artificial light-harvesting systems are restrained to the inevitable short fluorescence lifetimes of donor chromophores, which limit their practical application, such as time-resolved luminescence imaging that can eliminate the background signals of autofluorescence or scattered lights.[7] Therefore, it is highly desirable to discover alternative long-lived emitters as suitable donors to perform energy transfer process.

To this end, organic room-temperature phosphorescence (RTP) featuring longer emission lifetime and larger Stokes shift because of involving intersystem crossing (ISC), is identified as ideal candidate to address above issues.[8] Based on this, RTP energy transfer system has gradually become a new growth point, which can allow for the long lifetime of commercial fluorescent acceptors via a delayed sensitization process, showing great application prospect in biolabeling,[9] information security,[10] and stimulus-responsive materials.[11] In particular, a supramolecular strategy including host–guest complexation and assembly-induced emission has been demonstrated to be a feasible approach to realize efficient purely organic aqueous RTP emission and then conduct phosphorescence energy transfer.[12] For example, George et al. reported an efficient light-harvesting supramolecular phosphor scaffold in water, which achieved energy-transfer-mediated long-lived delayed fluorescence after the introduction of sulforhodamine acceptor dyes.[13] To date, although considerable endeavors have been undertaken to develop RTP energy transfer systems, near-infrared (NIR) emissive supramolecular phosphorescence-harvesting system concurrently featuring cancer cell-targeted imaging capacity and long lifetime performance is still rare in aqueous solution.

In this work, we constructed a noncovalent confinement assembly consisting of a dodecyl-chain-bridged 6-bromoisoquinoline derivative (abbreviated as G), cucurbit[7]uril (abbreviated

X.-Y. Dai, M. Huo, X. Dong, Y.-Y. Hu, Y. Liu
College of Chemistry
State Key Laboratory of Elemento-Organic Chemistry
Nankai University
Tianjin 300071, P. R. China
E-mail: yuliu@nankai.edu.cn

The ORCID identification number(s) for the author(s) of this article can be found under https://doi.org/10.1002/adma.202203534.

DOI: 10.1002/adma.202203534

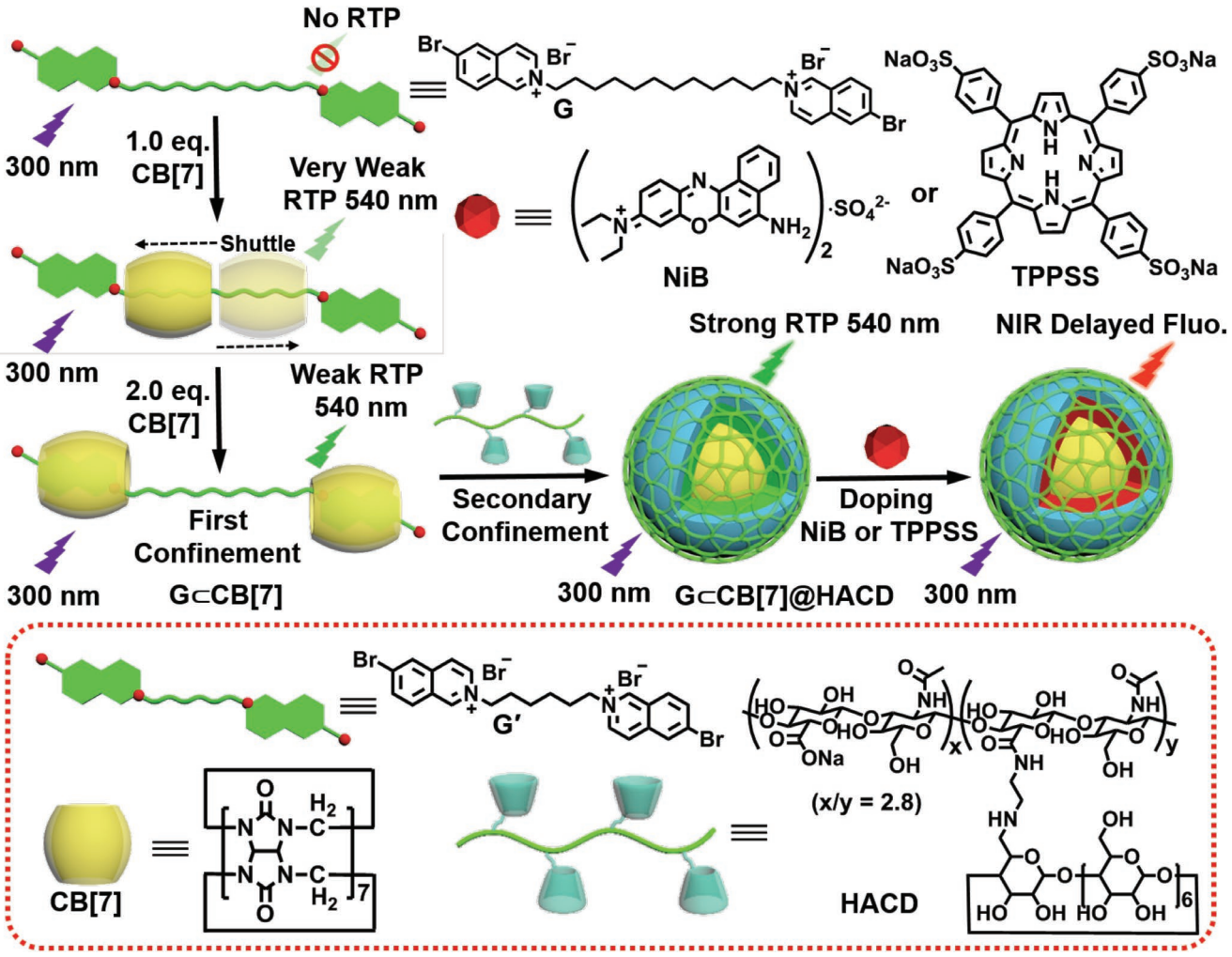

Scheme 1. Schematic illustration of the construction of polysaccharide supramolecular RTP-harvesting system with NIR emission in aqueous solution and corresponding chemical structures of the compounds used.

as CB[7]), and β-cyclodextrin-grafted hyaluronic acid (abbreviated as HACD), with the final goal of achieving high-efficiency supramolecular phosphorescence-harvesting process and demonstrating its potential applicability for NIR cancer cell-targeted imaging (**Scheme 1**). Specifically, benefitting from the first confinement effect of CB[7], phosphor G gave an emerging phosphorescence at 540 nm after the formation of dumbbell-shaped assembly G⊂CB[7]. Next, the noncovalent polymerization of such binary assembly enabled by HACD facilitated the enhancement of original phosphorescence intensity approximately eight times and lifetime from 59.0 µs to 0.581 ms due to the secondary confinement of HACD. Intriguingly, the long-lived NIR-emissive phosphorescence-harvesting system can be easily acquired after introduction of two different organic dyes Nile blue (NiB) or tetrasodium 5,10,15,20-tetrakis(4-sulfophenyl)porphyrin (TPPSS) as an acceptor into the G⊂CB[7]@HACD coassembly by virtue of the sufficient overlap between the absorption band of NiB or TPPSS and the phosphorescence emission band. Ultimately, due to the overexpressed HA receptors on the surface of cancer cells, the final assemblies were able to target cancer cells and especially achieve lysosome NIR imaging.

2. Results and Discussion

Two types of 6-bromoisoquinoline derivatives were selected as phosphorescent guest molecules in which the N-termini were, respectively, bridged with hexyl chain (abbreviated as G′) or dodecyl chain (abbreviated as G) to endow the molecules with diverse amphipathy. The specific synthetic routes of the two molecules and their detailed characterizations including ^{1}H NMR, ^{13}C NMR, and HR-MS (Figures S1–S7, Supporting Information) are supplied in the Supporting Information. ^{1}H NMR titration experiments were first performed to reveal the host–guest binding mode between CB[7] and G′ or G. As shown in Figure S9, Supporting Information, upon increasing the amount of CB[7] from 0 to 1.0 equivalent into the aqueous solution of G′, all hexyl-chain protons (H_g–H_i) gradually shifted upfield due to the shielding effect, while the aromatic protons (H_a–H_f) of the isoquinoline moiety slightly shifted downfield, indicating that the hexyl-chain part was deeply included in the cavity of CB[7] and isoquinoline moiety was located outside of CB[7].[14] However, when >1.0 equivalent CB[7] was added, the aromatic protons underwent obvious upfield shifts

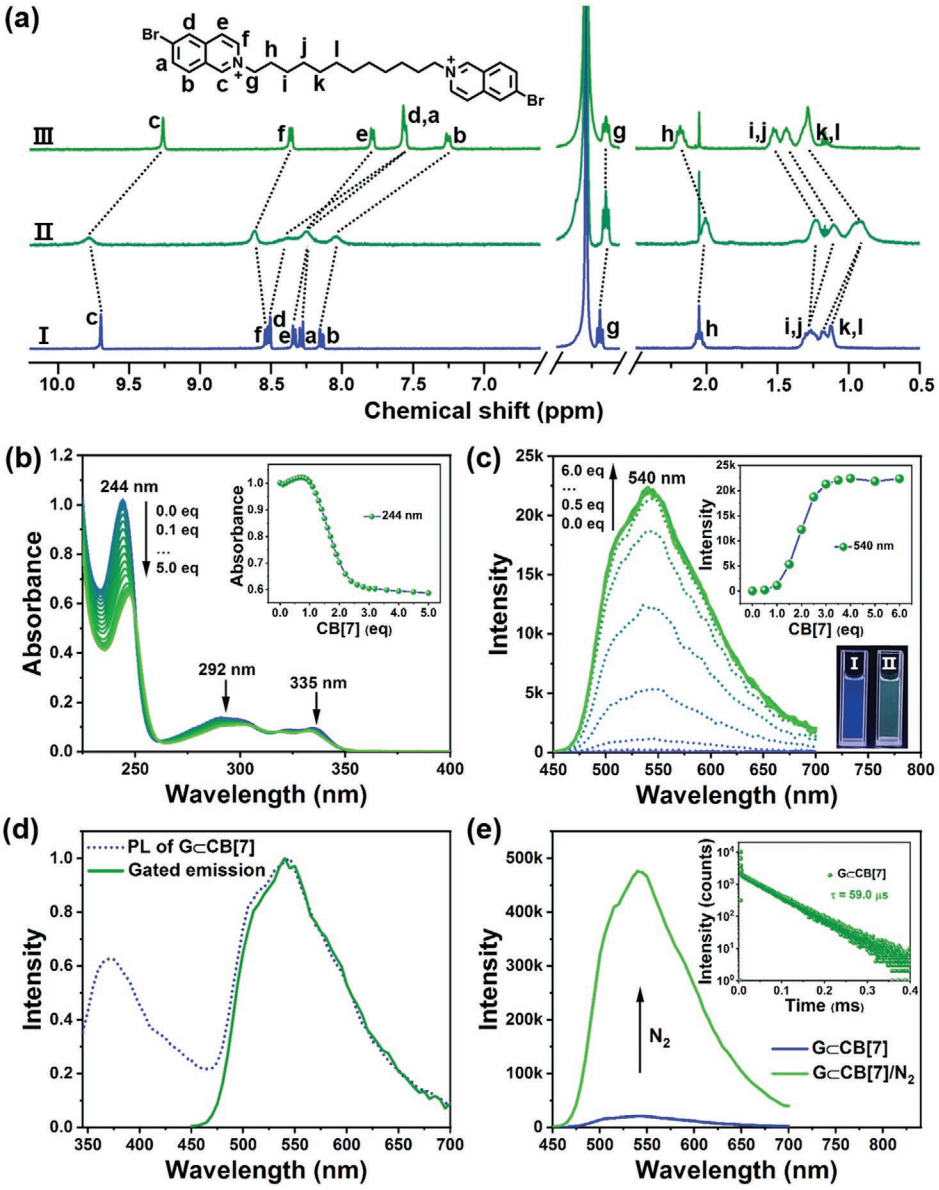

Figure 1. a) Partial ^{1}H NMR spectra (400 MHz, D_2O, 298 K) of G ([G] = 1.0×10^{-3} M) with 0 (I), 1.2 (II), and 4.0 (III) equivalents of CB[7]. b) UV–vis absorption spectra of G in water upon the gradual addition of CB[7] at 298 K ([G] = 1.0×10^{-5} M and [CB[7]] = 0–5.0×10^{-5} M). Inset: Absorbance intensity changes of G at 244 nm. c) Phosphorescence emission spectra (delay = 50 μs) of G at 540 nm in water upon the addition of 0, 0.5, 1.0, 1.5, 2.0, 2.5, 3.0, 3.5, 4.0, 5.0, and 6.0 equivalents of CB[7] at 298 K ([G] = 1.0×10^{-5} M, λ_{ex} = 300 nm). Inset: Phosphorescence emission intensity changes of G at 540 nm. Photograph of the aqueous solutions of free G (I) and G⊂CB[7] (II) upon illumination with UV light under ambient conditions. d) Normalized prompt photoluminescence spectrum and gated emission spectrum (delay 50 μs) of G⊂CB[7] in water at 298 K. e) Phosphorescence emission spectra (delay 50 μs) of G⊂CB[7] in water before and after N_2 bubbling at 298 K ([G] = 1.0×10^{-5} M, [CB[7]] = 3.0×10^{-5} M, λ_{ex} = 300 nm). Inset: Time-resolved photoluminescence decay spectrum of G⊂CB[7] at 540 nm in water at 298 K.

concurrently accompanied by significant downfield shifts of hexyl-chain protons, revealing that CB[7] moved from hexyl chain to isoquinoline part to form the dumbbell-shaped structure. All proton chemical shifts remained basically unchanged when the amount of CB[7] increased to >2.0 equivalents, confirming the 1:2 binding mode for G′⊂CB[7]. Similarly, protons of G went through a similar process (**Figure 1**a and Figure S10, Supporting Information). All the dodecyl-chain protons (H_g–H_l) first moved upfield with the gradual addition of CB[7] up to 1.2 equivalents, implying that the dodecyl chain docked to CB[7] via hydrophobic interactions and CB[7] shuttled rapidly on it. Then, upon increase of the CB[7] concentration to 2.0 equivalents, dodecyl-chain protons exerted a downfield shift while the aromatic protons exhibited a noticeable upfield shift, suggesting the tight encapsulation of isoquinoline moiety by CB[7] in virtue of the good binding affinity of CB[7] with isoquinolinium group.[15] Notably, both bound and free guest molecules could be simply discriminated on the ^{1}H NMR time scale

because of the slow exchange equilibria for the molecular recognition between CB[7] and G′. In contrast, fast exchange equilibria were found in the molecular recognition process between CB[7] and G. The possible binding mode between CB[7] and G is shown in Scheme 1.

Next, the CB[7]-confined optical properties of the host–guest complexes including G⊂CB[7] and G′⊂CB[7] were, respectively, investigated in aqueous solution. As shown in Figure 1b, three major absorption peaks at 244, 292, and 335 nm were observed for free G, which all showed a certain wavelength shift and intensity change upon the stepwise addition of CB[7]. Notably, there were two obvious inflection points for the absorbance intensity changes at 244 nm which were approximately located at the addition of 1.0 and 2.0 equivalents CB[7], also indicative of the change of host–guest inclusion mode in such addition process (Figure 1b, inset). Similar absorbance intensity changes can also be found in the process of addition CB[7] into G′ aqueous solution (Figure S11, Supporting Information). According to the UV–vis titrations, a two-stage binding process occurred during titration of G′ or G with CB[7], implying the final formation of a stable 1:2 host–guest complex (Figure S12, Supporting Information). Initially, CB[7] was located at the non-chromophore part dodecyl-chain of G or G′ within 0–1.0 eq, and then gradually moved to the chromophore isoquinoline part when more than 1.0 eq. Therefore, by using a nonlinear curve-fitting method, the association constant (K_a) was calculated to be 1.75×10^5 and 7.99×10^5 M^{-1}, respectively (Figure S13, Supporting Information). In the photoluminescence spectra, upon the continuous addition of CB[7], the original emission of G at ≈385 nm declined along with a remarkable increase for the new emission peak at 540 nm (Figure S14, Supporting Information). Different from the photoluminescence spectra, there was only one emission peak centered on 540 nm in the gated spectrum (Figure 1d, delay time = 50 μs), illustrating its long-lived feature. The gated emission spectrum revealed that the emission at 540 nm were almost silent in the presence of 0–1.0 equivalent of CB[7]; however, this emission gradually emerged and increased upon the further addition of CB[7], whose intensity began to level off when adding 3.0 equivalents of CB[7] simultaneously with the color change from initial blue to green under UV light irradiation (Figure 1c). According to the time-resolved decay profiles, the emission collected at 385 nm and 540 nm gave an average lifetime of 1.15 ns and 59.0 μs, respectively (Figure S15, Supporting Information, and Figure 1e, inset). Moreover, after the introduction of N_2 into the aqueous solution of G⊂CB[7], the emission intensity at 540 nm was greatly enhanced and the corresponding lifetime increased to 0.732 ms because of the avoidance of triplet electron quenching caused by oxygen, confirming the phosphorescence nature of emission at 540 nm (Figure 1e and Figure S16, Supporting Information). For G′, the addition of CB[7] from 0 to 1.0 equivalent barely induced any phosphorescence, hinting the invalid encapsulation of CB[7] toward isoquinoline part (Figure S17, Supporting Information). Continuing to add CB[7] to 3.0 equivalents, the phosphorescence intensity gradually increased and reached equilibrium. Based on the above experimental results, we can deduce that in the presence of 1.0 equivalent of CB[7], the guest molecule hardly produced any phosphorescent emission because CB[7] wrapped in the alkyl chain part. When the equivalent of CB[7] further increased, CB[7] moved to the isoquinoline part, which was conducive to the restriction of the phosphor motion and reduction of the non-radiative decay thereby resulting in effective phosphorescence due to the confinement effect of rigid cavity.

Recently, the secondary assembly strategy by using functional macrocyclic molecules has evolved into an important method to enhance the luminescence performance, especially for phosphorescent emission.[16] Therefore, after clarifying the CB[7]-confined phosphorescence emission, HACD was introduced to further co-assemble with G⊂CB[7] by virtue of its excellent water solubility, biocompatibility, and biodegradability. The substitution degree of the β-cyclodextrin (β-CD) was determined to be as 26.4% by comparing the integral area of the N-acetyl protons (H_b) of HA at 1.97 ppm with that of the H_1 proton of β-CD at 5.04 ppm (Figure S7, Supporting Information). And the molecular weight of HACD was calculated as 1.73×10^5 under this substitution degree based on the ^{1}H NMR spectrum, which was basically in coincidence with the weight-average molecular weight determined by gel permeation chromatography as 1.91×10^5 (Figure S8, Supporting Information). As depicted in **Figure 2**a, the phosphorescence intensity of G⊂CB[7] at 540 nm was gradually enhanced with the stepwise addition of HACD, which was almost in equilibrium when increasing the amount of HACD to 0.32 mg mL^{-1}. Ultimately, the original phosphorescence intensity was improved approximately eight times, and the phosphorescence lifetime was greatly extended from 59.0 μs to 0.581 ms (Figure 2b). The photoluminescence spectra also displayed similar results (Figure S18, Supporting Information). And the lifetime of emission at 385 nm was determined to be 1.73 ns (Figure S19, Supporting Information). Moreover, the aqueous solution of G⊂CB[7]@HACD emitted greater bright green phosphorescence than G⊂CB[7] under UV light irradiation (Figure 2a, inset). In addition, compared with G⊂CB[7] whose phosphorescence quantum yield was 1.15%, the phosphorescence quantum yield of G⊂CB[7]@HACD was dramatically increased to 10.42% (Figure S20, Supporting Information). It was worth noting that the co-assembly between G and HACD cannot generate any phosphorescence (Figure S21, Supporting Information), thereby indicating that the confinement effect of CB[7] toward G performed an extremely important role in inducing phosphorescence, elaborating that the addition of HACD would indeed improve the phosphorescent performance rather than destroying the G⊂CB[7] complex. Based on the measured lifetimes and quantum yields of G⊂CB[7] and G⊂CB[7]@HACD, the ISC rate constants (k_{isc}) and the quantum yields of ISC (Φ_{isc}) could be calculated according to the standard methods,[12b] where the k_{isc} and Φ_{isc} of G⊂CB[7]@HACD were 6.02×10^7 S^{-1} and 0.12, respectively, which were higher than that of G⊂CB[7] (1.00×10^7 S^{-1} and 0.013), indicating that G⊂CB[7]@HACD displayed an enhanced ISC process (Table S1, Supporting Information).

In control experiments, the addition bare HA into G⊂CB[7] solution cannot obviously enhance phosphorescence intensity and phosphorescence lifetime like HACD, highlighting the important role of β-CD in secondary assembly process (Figures S22 and S23, Supporting Information). In order to further investigate the influence of aliphatic chain length of guest molecules on secondary assembly-induced optical changes, ^{1}H

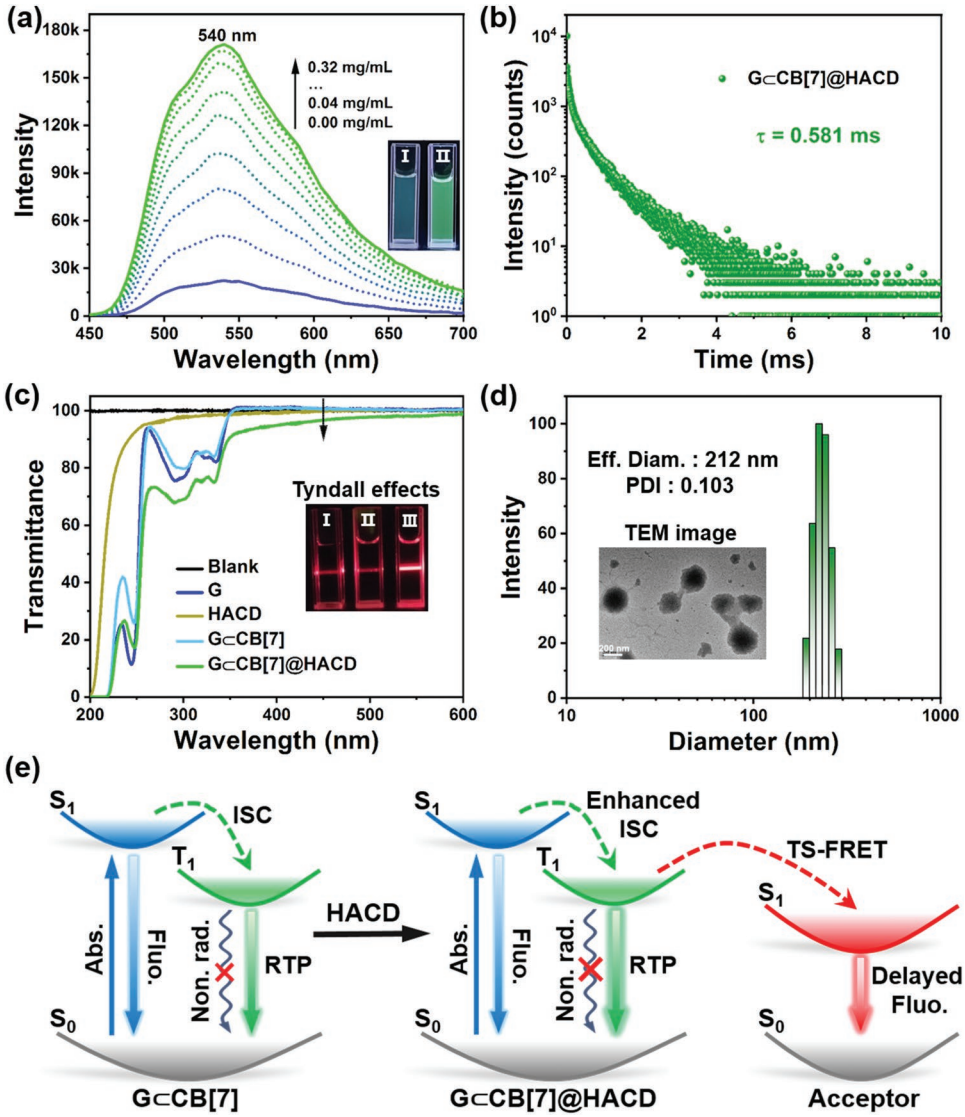

Figure 2. a) Phosphorescence emission spectra (delay = 50 µs) of G⊂CB[7] at 540 nm upon the addition of 0, 0.04, 0.08, 0.12, 0.16, 0.20, 0.24, 0.28, and 0.32 mg mL^{-1} of HACD in water at 298 K ([G] = 1.0×10^{-5} M, [CB[7]] = 3.0×10^{-5} M, λ_{ex} = 300 nm). Inset: Photographs of the aqueous solutions of G⊂CB[7] (I) and G⊂CB[7]@HACD (II) upon illumination with UV light under ambient conditions. b) Time-resolved photoluminescence decay spectrum of G⊂CB[7]@HACD at 540 nm in water at 298 K. c) The optical transmittance of G, HACD, G⊂CB[7], and G⊂CB[7]@HACD at 450 nm in water ([G] = 1.0×10^{-5} M, [CB[7]] = 3.0×10^{-5} M, [HACD] = 0.32 mg mL^{-1}). Inset: Tyndall effects of G (I), G⊂CB[7] (II), and G⊂CB[7]@HACD (III). d) Size distribution determined by scattered light intensity of G⊂CB[7]@HACD measured by dynamic light scattering. Inset: Transmission electron microscopy image of G⊂CB[7]@HACD in water. e) Diagram of the possible mechanism for supramolecular RTP energy transfer process (Abs. = absorption, Fluo. = fluorescence, Non. rad. = non-radiation, ISC = intersystem crossing, TS-FRET = triplet-to-singlet Förster resonance energy transfer).

NMR experiments were first performed by using β-CD as a reference host. All protons assigned to G′ showed no obvious chemical shifts for G′ or G′⊂CB[7] upon addition of β-CD, proving that there was no interaction between β-CD and them (Figure S24, Supporting Information). Similar phenomenon could also be observed for bare G after the addition of β-CD (Figure S25a,b, Supporting Information). Conversely, the dodecyl-chain protons for G⊂CB[7] underwent a significant downfield shift, verifying that the hydrophobic dodecyl chain that could function as binding site for β-CD (Figure S25c,d, Supporting Information).[17] The different chemical shifts between β-CD and G or G⊂CB[7] were probably derived from the shielding of positive charge part of G after encapsulation with CB[7] which was beneficial to the interaction between dodecyl chain and β-CD. Similarly, upon the addition of HACD into G⊂CB[7], an obvious downfield shift of the dodecyl-chain protons for G⊂CB[7] was found (Figure S26, Supporting Information), directly confirming the co-assembly process owing to the multivalent interactions. Moreover, G′⊂CB[7] was also utilized to co-assemble with HACD for comparison. The original phosphorescence emission of G′⊂CB[7] showed an overall downward trend after gradual addition of HACD under the same experimental conditions (Figure S27, Supporting Information). And the phosphorescence lifetime of G′⊂CB[7] was roughly comparable to

that of G′⊂CB[7]@HACD, which were measured as 0.137 and 0.149 ms, respectively (Figures S28 and S29, Supporting Information). These experimental results consistently indicated that the possession of longer aliphatic chain length for G could provide extra binding sites to assemble with β-CD due to the hydrophobic interaction, which further facilitated the secondary assembly process between G⊂CB[7] and HACD. The excellent phosphorescent performance of G⊂CB[7]@HACD was mainly ascribed to the stepwise encapsulation of the part of hydrophobic dodecyl chain by β-CD cavity and the subsequent noncovalent polymerization effect enabled by HACD, thereby leading to the formation of multivalent interactions including hydrophobic interaction, electrostatic attraction interactions, and multiple hydrogen bonding interactions, and ultimately achieving the further inhibition of non-radiative relaxation attenuation and the generation of hydrophobic environment after secondary assembly that protected the phosphor from attack of dissolved oxygen species.

Additionally, the changes of optical transmittance in such assembly process were also monitored. Compared with blank sample (pure water), there were no obvious changes of optical transmittance for free G, HACD, and G⊂CB[7]; however, the optical transmittance of G⊂CB[7] at 450 nm dramatically decreased after the subsequent assembly with HACD (Figure 2c). Both G and G⊂CB[7] showed slight Tyndall effect, whereas an obvious Tyndall effect can be found for G⊂CB[7]@HACD, further indicative of the existence of large assemblies (Figure 2c, inset). Subsequently, dynamic light scattering (DLS), transmission electron microscopy (TEM), and zeta potential experiments were carried out to explore the specific morphologic structure after the co-assembly of G⊂CB[7] and HACD. DLS measurements suggested that G⊂CB[7]@HACD assemblies had an average hydrodynamic diameter of 212 nm with a narrow size distribution (Figure 2d). Besides, according to the number distribution of particles, the majority of obtained assemblies were ≈224 nm in diameter while the free HACD showed diameter from 100 to 1000 nm (Figures S30 and S31, Supporting Information). The TEM images of G⊂CB[7] showed a number of small irregular nanoaggregates, while G⊂CB[7]@HACD presented as numerous solid spherical nanoparticles with a diameter ranging from 200 to 220 nm, which matched well with the DLS results (Figure S32, Supporting Information, and Figure 2d, inset). Moreover, in contrast with G⊂CB[7] with a positive zeta potential as 39.1 mV, a negative surface potential value (−30.2 mV) was observed for G⊂CB[7]@HACD, implying the distribution of anionic HACD on the surface of nanoparticles (Figure S33, Supporting Information). Combining above experimental results, we proved that the binary complex G⊂CB[7] can definitely further continue to co-assemble with HACD to form homogeneous nanoparticles benefiting from the multivalent interactions consisting of hydrogen-bond, electrostatic, and hydrophobic interactions.

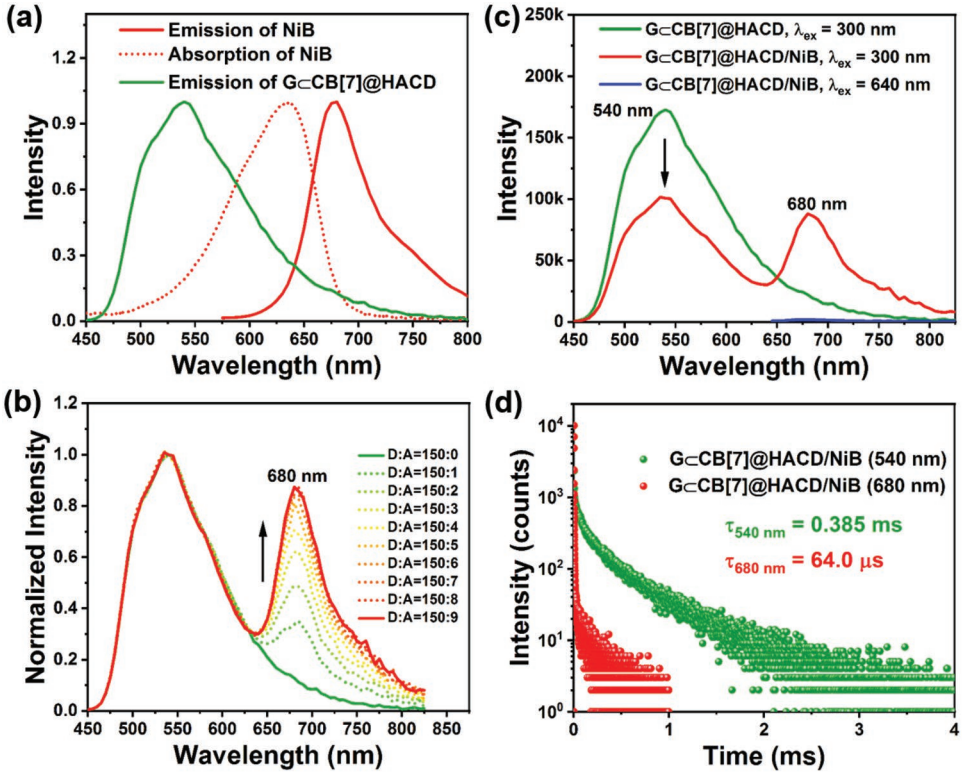

Figure 3. a) Normalized phosphorescence emission spectrum of G⊂CB[7]@HACD, and the absorption and emission spectra of NiB. b) Phosphorescence emission spectra of G⊂CB[7]@HACD with increasing the doping concentration of NiB in water based on the normalization of phosphorescence emission peak at 540 nm. c) Phosphorescence emission spectra of G⊂CB[7]@HACD (λ_{ex} = 300 nm), G⊂CB[7]@HACD/NiB (λ_{ex} = 300 nm), and G⊂CB[7]@HACD/NiB (λ_{ex} = 640 nm) in water ([G] = 1.0×10^{-5} M, [CB[7]] = 3.0×10^{-5} M, [HACD] = 0.32 mg mL^{-1}, [NiB] = 6.0×10^{-7} M). d) Time-resolved photoluminescence decay spectra of G⊂CB[7]@HACD/NiB at 540 and 680 nm in water at 298 K.

Subsequently, given that G⊂CB[7]@HACD assembly possessed excellent RTP performance and inner hydrophobic layer, it might serve as a potential RTP-harvesting platform by loading suitable dye molecules into the assembly. An NIR emissive organic dye NiB with positive charge was adopt as the acceptor to probe the phosphorescence energy transfer process as a result of a clear spectral overlap between the RTP emission band of G⊂CB[7]@HACD and the absorption band of NiB (**Figure 3**a). When NiB was added into the aqueous solution of G⊂CB[7]@HACD with the donor/acceptor ratio of 150:1, an emerging NIR emission at 680 nm was observed in the gated spectra (Figure 3b). Moreover, upon increasing donor/acceptor ratio from 150:1 to 150:9, the phosphorescence emission of donor intensity at 540 nm was gradually quenched accompanied by a concomitant enhancement of NIR emission intensity with a phosphorescence quantum yield of 14.96% (Figure 3c and Figure S34a, Supporting Information). Time-resolved decay measurements showed that the phosphorescence lifetime at 540 nm decreased from 0.581 to 0.385 ms, further indicating the occurrence of phosphorescence energy process (Figure 3d). Accordingly, the efficiency of energy transfer (Φ_{ET}) was calculated to be 34% based on the decreased donor lifetime. Interestingly, the lifetime of this gated NIR emission from the final G⊂CB[7]@HACD/NiB system was a microsecond lifetime as 64.0 µs, while the HACD/NiB exhibited a nanosecond lifetime as 1.95 ns (Figure 3d and Figure S35, Supporting Information). And such gated emission peak was consistent with the fluorescence emission of bare NiB, demonstrating its characteristic NIR delayed fluorescence emission. In addition, negligible delayed fluorescence emission was detected when selectively exciting G⊂CB[7]@HACD/NiB system with the optimal wavelengths of NiB at 640 nm (Figure 3c). These results clearly illustrated that the high-efficiency RTP energy transfer took place within the assembly based on the delayed sensitization process from triplet of G⊂CB[7]@HACD to singlet of NiB via the FRET mechanism.[18]

In order to verify that G⊂CB[7]@HACD can function as a general phosphorescence-harvesting platform, another anionic dye TPPSS was also selected as a receptor to explore the possibility of RTP energy transfer. Although G⊂CB[7]@HACD assembly showed negative zeta potential, a small amount of anionic dye TPPSS can be still loaded into assembly on account of the host–guest interaction between β-CD and TPPSS.[19] TPPSS showed a sharp peak at 412 nm and a broad absorption in the 450–700 nm range, which were assigned to the Soret band and Q-band, respectively (Figure S36, Supporting Information). Notably, all the Q-band absorptions fall into the RTP emission band of G⊂CB[7]@HACD, suggesting an efficient RTP energy transfer process could occur (**Figure 4**a). In the gated spectra, the RTP emission peak at 540 nm markedly declined upon continuous addition of TPPSS with the donor/acceptor ratio from 150:1 to 150:12, while two new peaks at 645 and 710 nm

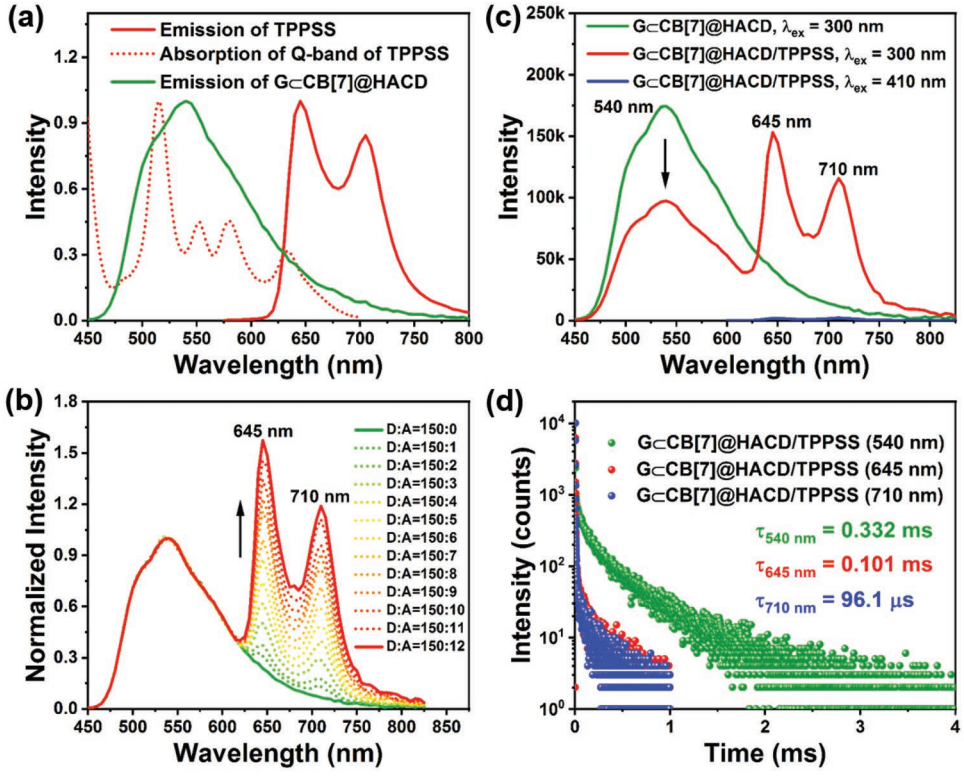

Figure 4. a) Normalized phosphorescence emission spectrum of G⊂CB[7]@HACD, and the *Q*-band absorption and emission spectra of TPPSS. b) Phosphorescence emission spectra of G⊂CB[7]@HACD with increasing the doping concentration of TPPSS in water based on the normalization of phosphorescence emission peak at 540 nm. c) Phosphorescence emission spectra of G⊂CB[7]@HACD (λ_{ex} = 300 nm), G⊂CB[7]@HACD/TPPSS (λ_{ex} = 300 nm), and G⊂CB[7]@HACD/TPPSS (λ_{ex} = 410 nm) in water ([G] = 1.0×10^{-5} M, [CB[7]] = 3.0×10^{-5} M, [HACD] = 0.32 mg mL^{-1}, [TPPSS] = 8.0×10^{-7} M). d) Time-resolved photoluminescence decay spectra of G⊂CB[7]@HACD/TPPSS at 540, 645, and 710 nm in water at 298 K.

corresponding to the characteristic emission peaks of TPPSS formed at the same time and the phosphorescence quantum yield was determined to be 16.74% after energy transfer process (Figure 4b,c and Figure S34b, Supporting Information). No appreciable delayed emission of G⊂CB[7]@HACD/TPPSS was observed when directly excited at 410 nm (Figure 4c). The phosphorescence lifetime at 540 nm was shortened to 0.332 ms according to the time-resolved decay curves and the Φ_{ET} was calculated to be 43% (Figure 4d). Importantly, the lifetimes at 645 and 710 nm for G⊂CB[7]@HACD/TPPSS were found to be 0.101 ms and 96.1 µs, respectively, which were distinctly longer than the lifetimes of HACD/TPPSS that located at nanosecond level as 9.66 and 7.62 ns (Figure S37, Supporting Information). These phenomena undoubtedly demonstrated the efficient phosphorescence energy transfer process from the triplet state of G⊂CB[7]@HACD to the singlet state of TPPSS. The possible mechanism for such supramolecular RTP energy transfer process is presented in Figure 2e.

In the light of the excellent delayed NIR emission performance of such supramolecular phosphorescence-harvesting system, the targeted imaging of cancer cells is attempted to illustrate its potential applicability by taking G⊂CB[7]@HACD/NiB as an example. Two types of cancer cells including human lung adenocarcinoma cells (A549 cells) and human cervical carcinoma cells (HeLa cells) were, respectively, incubated with G⊂CB[7]@HACD/NiB for 24 h, followed by the visualization of intracellular NIR emission signal utilizing confocal laser scanning microscopy. As shown in **Figure 5**, both of these two cancer cells exhibited bright red signal in the cytoplasm and evenly distributed around the nucleus, whereas almost no red emission signal was found for normal human embryonic kidney cells (293T cells). These imaging results implied that G⊂CB[7]@HACD/NiB was preferentially internalized by cancer cells than normal cells by virtue of the HA receptor mediated-endocytosis.[20] Compared with the traditional cell dyes, such phosphorescence energy transfer system concurrently possesses NIR-emissive property and long microsecond-scale lifetime, which would avoid the interference from background fluorescence or autofluorescence for cell imaging. In addition, the subcellular localization of such supramolecular assembly was probed by employing a commercial lysosome marker LysoTracker Green. The co-localization analysis revealed that the NIR red luminescence signal overlapped well with the green signal of LysoTracker Green as indicated by the emergence of

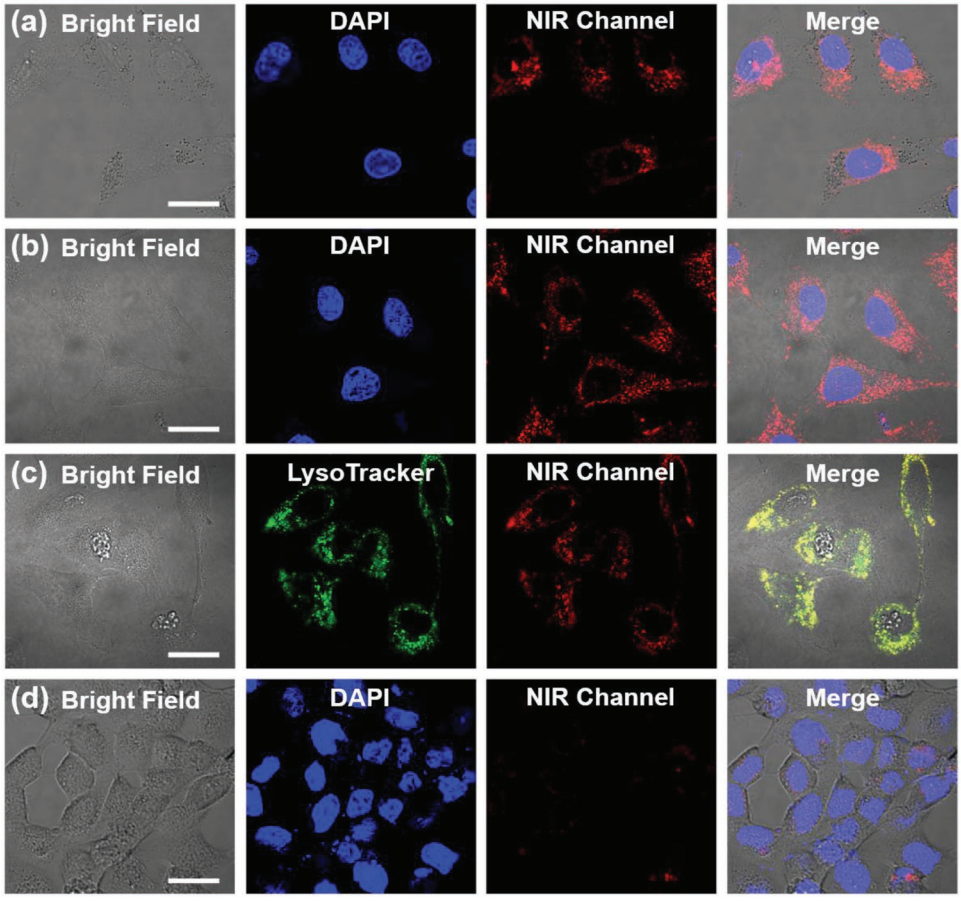

Figure 5. a,b,d) Cellular imaging of A549 cancer cells (a), HeLa cancer cells (b), and 293T normal cells (d) after co-staining with the G⊂CB[7]@HACD/NiB assembly ([G] = 1.0×10^{-5} M, [CB[7]] = 3.0×10^{-5} M, [HACD] = 0.32 mg mL^{-1}, [NiB] = 6.0×10^{-7} M). c) Lysosomes co-localization images of G⊂CB[7]@HACD/NiB in living A549 cancer cells. The nuclei were stained by 4,6-diamidino-2-phenylindole (DAPI, blue), which was collected from 420 to 470 nm. The lysosomes were stained by commercial LysoTracker Green, which was collected from 500 to 550 nm. The NIR channel was collected from 650 to 700 nm (Scale bar = 20 µm).

yellow areas in the merged image, simultaneously presenting a high Pearson's correlation coefficient of 0.88 in A549 cells (Figure 5c and Figure S38, Supporting Information). In addition, the cytotoxicity of such assembly was also evaluated via Cell Counting Kit-8 assay. The assay results displayed that the viability of these three kinds of cells could all still keep above 92% after 24 h incubation with G⊂CB[7]@HACD/NiB ranging from 0 to 40×10^{-6} M, indicative of its relatively low cellular toxicity (Figure S39, Supporting Information). These results illustrated that G⊂CB[7]@HACD/NiB not only had low cytotoxicity, but also possessed specific lysosome-targeting ability of cancer cells, which had potential application in NIR imaging of living cells for biological research.

3. Conclusion

An aqueous-phase supramolecular phosphorescence-harvesting system was successfully constructed by the cascaded assembly of G, CB[7], and HACD, which ultimately achieved long-lived NIR emission by doping a small amount of NiB or TPPSS and successfully being applied in targeted imaging of cancer cells. The first confinement of CB[7] promoted the ISC of G due to the strong host–guest complexation, meanwhile the secondary confinement of HACD derived from the noncovalent polymerization further synergistically suppressed the non-radiative transition and finally contributed to efficient phosphorescent performance because of the formation of multivalent interactions. Significantly, benefiting from the delayed sensitization process, the efficient phosphorescence energy transfer endowed the doped organic dyes with long-lived NIR feature, thereby making it suitable for NIR targeted imaging of cancer cells. This study not only contributes to the construction of phosphorescence-harvesting system concurrently accompanied by long-lived NIR-emission performance and targeted biological function in aqueous solution, but also has potential application values in photocatalysis, chemical sensing, photodynamic therapy, and so forth.

Supporting Information

Supporting Information is available from the Wiley Online Library or from the author.

Acknowledgements

This work was financially supported by the National Natural Science Foundation of China (22131008 and 22101143).

Conflict of Interest

The authors declare no conflict of interest.

Data Availability Statement

The data that support the findings of this study are available from the corresponding author upon reasonable request.

Keywords

long-lived near-infrared emission, noncovalent polymerization, phosphorescence energy transfer, stepwise confinement, targeted imaging

Received: April 19, 2022
Revised: May 26, 2022
Published online:

[1] a) X. M. Chen, Q. Cao, H. K. Bisoyi, M. Wang, H. Yang, Q. Li, *Angew. Chem., Int. Ed.* **2020**, *59*, 10493; b) P. Wang, X. Miao, Y. Meng, Q. Wang, J. Wang, H. Duan, Y. Li, C. Li, J. Liu, L. Cao, *ACS Appl. Mater. Interfaces* **2020**, *12*, 22630; c) H. Nie, Z. Wei, X. L. Ni, Y. Liu, *Chem. Rev.* **2022**, *122*, 9032; d) X.-F. Hou, S. Zhang, X. Chen, H. K. Bisoyi, T. Xu, J. Liu, D. Chen, X.-M. Chen, Q. Li, *ACS Appl. Mater. Interfaces* **2022**, *14*, 22443.

[2] a) P. Ashokkumar, N. Adarsh, A. S. Klymchenko, *Small* **2020**, *16*, 2002494; b) Z. Liu, X. Sun, X. Dai, J. Li, P. Li, Y. Liu, *J. Mater. Chem. C* **2021**, *9*, 1958; c) N. Melnychuk, A. S. Klymchenko, *J. Am. Chem. Soc.* **2018**, *140*, 10856; d) T. Xiao, C. Bao, L. Zhang, K. Diao, D. Ren, C. Wei, Z.-Y. Li, X.-Q. Sun, *J. Mater. Chem. A* **2022**, *10*, 8528.

[3] a) Y.-N. Jing, S.-S. Li, M. Su, H. Bao, W.-M. Wan, *J. Am. Chem. Soc.* **2019**, *141*, 16839; b) L. Xu, Z. Wang, R. Wang, L. Wang, X. He, H. Jiang, H. Tang, D. Cao, B. Z. Tang, *Angew. Chem., Int. Ed.* **2019**, *59*, 9908; c) Y. Li, S. S. Rajasree, G. Y. Lee, J. Yu, J.-H. Tang, R. Ni, G. Li, K. N. Houk, P. Deria, P. J. Stang, *J. Am. Chem. Soc.* **2021**, *143*, 2908; d) Z. Yu, H. K. Bisoyi, X. M. Chen, Z. Z. Nie, M. Wang, H. Yang, Q. Li, *Angew. Chem., Int. Ed.* **2022**, *134*, e202200466.

[4] a) M. Hao, G. Sun, M. Zuo, Z. Xu, Y. Chen, X. Y. Hu, L. Wang, *Angew. Chem., Int. Ed.* **2019**, *59*, 10095; b) A. Kumar, R. Saha, P. S. Mukherjee, *Chem. Sci.* **2021**, *12*, 5319; c) W. J. Li, X. Q. Wang, D. Y. Zhang, Y. X. Hu, W. T. Xu, L. Xu, W. Wang, H. B. Yang, *Angew. Chem., Int. Ed.* **2021**, *60*, 18761; d) Y. Sun, F. Guo, T. Zuo, J. Hua, G. Diao, *Nat. Commun.* **2016**, *7*, 12042; e) Z. Zhang, Z. Zhao, Y. Hou, H. Wang, X. Li, G. He, M. Zhang, *Angew. Chem., Int. Ed.* **2019**, *58*, 8862.

[5] a) H.-Q. Peng, L.-Y. Niu, Y.-Z. Chen, L.-Z. Wu, C.-H. Tung, Q.-Z. Yang, *Chem. Rev.* **2015**, *115*, 7502; b) S. Fu, X. Su, M. Li, S. Song, L. Wang, D. Wang, B. Z. Tang, *Adv. Sci.* **2020**, *7*, 2001909; c) K. Wang, K. Velmurugan, B. Li, X.-Y. Hu, *Chem. Commun.* **2021**, *57*, 13641.

[6] a) J.-J. Li, Y. Chen, J. Yu, N. Cheng, Y. Liu, *Adv. Mater.* **2017**, *29*, 1701905; b) S. Guo, Y. Song, Y. He, X.-Y. Hu, L. Wang, *Angew. Chem., Int. Ed.* **2018**, *57*, 3163; c) X. H. Wang, N. Song, W. Hou, C. Y. Wang, Y. Wang, J. Tang, Y. W. Yang, *Adv. Mater.* **2019**, *31*, 1903962; d) X.-M. Chen, S. Zhang, X. Chen, Q. Li, *ChemPhotoChem* **2022**, 4, e202100256.

[7] a) Y. X. Hu, W. J. Li, P. P. Jia, X. Q. Wang, L. Xu, H. B. Yang, *Adv. Opt. Mater.* **2020**, *8*, 2000265; b) X.-M. Chen, X.-F. Hou, H. K. Bisoyi, W.-J. Feng, Q. Cao, S. Huang, H. Yang, D. Chen, Q. Li, *Nat. Commun.* **2021**, *12*, 4993; c) F. Xiao, H. Gao, Y. Lei, W. Dai, M. Liu, X. Zheng, Z. Cai, X. Huang, H. Wu, D. Ding, *Nat. Commun.* **2022**, *13*, 186;

[8] a) A. D. Nidhankar, V. C. W. Goudappagouda, S. S. Babu, *Chem. Sci.* **2021**, *12*, 4216; b) R. Gao, M. S. Kodaimati, D. Yan, *Chem. Soc. Rev.* **2021**, *50*, 5564; c) S. Guo, W. Dai, X. Chen, Y. Lei, J. Shi, B. Tong, Z. Cai, Y. Dong, *ACS Mater. Lett.* **2021**, *3*, 379; d) N. Gan, H. Shi, Z. An, W. Huang, *Adv. Funct. Mater.* **2018**, *28*, 1802657; e) J. Guo, C. Yang, Y. Zhao, *Acc. Chem. Res.* **2022**, *55*, 1160.

[9] a) M. Huo, X. Y. Dai, Y. Liu, *Angew. Chem., Int. Ed.* **2021**, *60*, 27171; b) Y.-C. Liang, Q. Cao, K.-K. Liu, X.-Y. Peng, L.-Z. Sui, S.-P. Wang, S.-Y. Song, X.-Y. Wu, W.-B. Zhao, Y. Deng, Q. Lou, L. Dong, C.-X. Shan, *ACS Nano* **2021**, *15*, 16242; c) L. Mo, H. Liu, Z. Liu, X. Xu, B. Lei, J. Zhuang, Y. Liu, C. Hu, *Adv. Opt. Mater.* **2022**, *10*, 2102666; d) Q. Dang, Y. Jiang, J. Wang, J. Wang, Q. Zhang, M. Zhang, S. Luo, Y. Xie, K. Pu, Q. Li, Z. Li, *Adv. Mater.* **2020**, *32*, 2006752.

[10] a) F. Lin, H. Wang, Y. Cao, R. Yu, G. Liang, H. Huang, Y. Mu, Z. Yang, Z. Chi, *Adv. Mater.* **2022**, *34*, 2108333; b) W.-W. Xu, Y. Chen, Y.-L. Lu, Y.-X. Qin, H. Zhang, X. Xu, Y. Liu, *Angew. Chem., Int. Ed.* **2022**, *61*, e202115265; c) B. Zhou, D. Yan, *Adv. Funct. Mater.* **2019**, *29*, 1807599; d) K. Hayashi, K. Fukasawa, T. Yamashita, S. Hirata, *Chem. Mater.* **2022**, *34*, 1627; e) W.-L. Zhou, W. Lin, Y. Chen, X.-Y. Dai, Z. Liu, Y. Liu, *Chem. Sci.* **2022**, *13*, 573.

[11] a) F. Gu, B. Ding, X. Ma, H. Tian, *Ind. Eng. Chem. Res.* **2020**, *59*, 1578; b) C. Wang, X.-K. Ma, P. Guo, C. Jiang, Y.-H. Liu, G. Liu, X. Xu, Y. Liu, *Adv. Sci.* **2022**, *9*, 2103041; c) D. Li, Y. Yang, J. Yang, M. Fang, B. Z. Tang, Z. Li, *Nat. Commun.* **2022**, *13*, 347; d) Y. Zhao, L. Ma, Z. Huang, J. Zhang, I. Willner, X. Ma, H. Tian, *Adv. Opt. Mater.* **2022**, *10*, 2102701; e) L. Ma, Q. Xu, S. Sun, B. Ding, Z. Huang, X. Ma, H. Tian, *Angew. Chem., Int. Ed.* **2022**, *61*, e202115748.

[12] a) X.-K. Ma, Y. Liu, *Acc. Chem. Res.* **2021**, *54*, 3403; b) T. Zhang, X. Ma, H. Wu, L. Zhu, Y. Zhao, H. Tian, *Angew. Chem., Int. Ed.* **2020**, *59*, 11206; c) X. Ma, J. Wang, H. Tian, *Acc. Chem. Res.* **2019**, *52*, 738; d) X. Yan, H. Peng, Y. Xiang, J. Wang, L. Yu, Y. Tao, H. Li, W. Huang, R. Chen, *Small* **2022**, *18*, 2104073; e) Y. Zhang, X. Chen, J. Xu, Q. Zhang, L. Gao, Z. Wang, L. Qu, K. Wang, Y. Li, Z. Cai, Y. Zhao, C. Yang, *J. Am. Chem. Soc.* **2022**, *144*, 6107.

[13] S. Garain, B. C. Garain, M. Eswaramoorthy, S. K. Pati, S. J. George, *Angew. Chem., Int. Ed.* **2021**, *60*, 19720.

[14] a) K. Moon, A. Kaifer, *Org. Lett.* **2004**, *6*, 185; b) L. Zhu, H. Yan, X.-J. Wang, Y. Zhao, *J. Org. Chem.* **2012**, *77*, 10168; c) Z.-J. Zhang, Y.-M. Zhang, Y. Liu, *J. Org. Chem.* **2011**, *76*, 4682; d) Y. Liu, X.-Y. Li, H.-Y. Zhang, C.-J. Li, F. Ding, *J. Org. Chem.* **2007**, *72*, 3640; e) L.-H. Wang, Z.-J. Zhang, H.-Y. Zhang, H.-L. Wu, Y. Liu, *Chin. Chem. Lett.* **2013**, *24*, 949.

[15] a) Y. Gong, H. Chen, X. Ma, H. Tian, *ChemPhysChem* **2016**, *17*, 1934; b) T. Li, X. Ma, *Dyes Pig.* **2018**, *148*, 306; c) X.-Y. Dai, Y.-Y. Hu, Y. Sun, M. Huo, X. Dong, Y. Liu, *Adv. Sci.* **2022**, *9*, 2200524.

[16] a) X.-M. Chen, Y. Chen, Q. Yu, B.-H. Gu, Y. Liu, *Angew. Chem., Int. Ed.* **2018**, *57*, 12519; b) Z. Liu, X. Dai, Y. Sun, Y. Liu, *Aggregate* **2020**, *1*, 31; c) Z. Xu, S. Peng, Y.-Y. Wang, J.-K. Zhang, A. I. Lazar, D.-S. Guo, *Adv. Mater.* **2016**, *28*, 7666; d) M. Huo, X. Y. Dai, Y. Liu, *Small* **2022**, *18*, 2104514.

[17] a) X. Wu, Y. Chen, Q. Yu, F.-Q. Li, Y. Liu, *Chem. Commun.* **2019**, *55*, 4343; b) J. Czescik, Y. Lyu, S. Neuberg, P. Scrimin, F. Mancin, *J. Am. Chem. Soc.* **2020**, *142*, 6837.

[18] a) R. Gao, D. Yan, *Chem. Sci.* **2017**, *8*, 590; b) A. Kirch, M. Gmelch, S. Reineke, *J. Phys. Chem. Lett.* **2019**, *10*, 310; c) S. Kuila, S. J. George, *Angew. Chem., Int. Ed.* **2020**, *59*, 9393.

[19] a) Y. Liu, K.-F. Ke, H.-Y. Zhang, J. Cui, D. Ding, *J. Am. Chem. Soc.* **2008**, *130*, 600; b) Y. Zhao, Y. Huang, H. Zhu, Q. Zhu, Y. Xia, *J. Am. Chem. Soc.* **2016**, *138*, 16645.

[20] a) S. Z. F. Phua, G. Yang, W. Q. Lim, A. Verma, H. Chen, T. Thanabalu, Y. Zhao, *ACS Nano* **2019**, *13*, 4742; b) X. Dai, B. Zhang, W. Zhou, Y. Liu, *Biomacromolecules* **2020**, *21*, 4998; c) S. Z. F. Phua, C. Xue, W. Q. Lim, G. Yang, H. Chen, Y. Zhang, C. F. Wijaya, Z. Luo, Y. Zhao, *Chem. Mater.* **2019**, *31*, 3349; d) W.-L. Zhou, Y. Chen, Q. Yu, H. Zhang, Z.-X. Liu, X.-Y. Dai, J.-J. Li, Y. Liu, *Nat. Commun.* **2020**, *11*, 4655.